Precursors_cci+

ESA Climate Change Initiative (CCI)

D5.1 Climate Assessment Report (CAR)

Title	D5.1 Climate Assessment Report (CAR)
Reference	Precursors_cci+_D5.1_CAR_01_02
Issue	01
Revision	02
Status	Draft
Date of issue	23/04/2024
Document type	Deliverable

This work has received funding from the European Space Agency under Contract No 4000138243 and is the result of the cooperation between the partners of the Precursors_cci+ consortium.

	FUNCTION	NAME	DATE
LEAD AUTHOR(S)	Scientist	Herizo Narivelo Brice Barret Folkert Boersma	23/04/2024
REVIEWED BY	Science Leaders	M. Van Roozendael Folkert Boersma	23/04/2023 23/04/2023
	ESA Project Officer	Simon Pinnock	../../….
DISTRIBUTED TO	ESA Precursors_cci+ Consortium		

DOCUMENT CHANGE RECORD

Issue	Revision	Date	Modified items	Observations
0	0	03/04/2024	Initial template	Creation of document
	2	23/04/2024	First draft	

Table of Contents

Executive Summary

This document presents the first issue of the Climate Assessment Report for cycle 1 of the ESA CCI+ ECV Precursor project. Within the first 18 months of the project, climate users have been obtaining an idea about the format, usefulness and quality of the climate data records that are being developed for the trace gases NO_2 and HCHO within the ECV Precursor project. We report on the views held by ECMWF and NASA-personnel involved in R&D for the development of long-term reanalyses of atmospheric composition on the (prototype) CDRs produced in the ESA CCI+ ECV Precursor project. The document further explains how a multi-year model simulation by GEOS-Chem with a focus on the Tropics has been prepared, how the first level-3 (monthly mean) records of OMI and TROPOMI NO_2 and HCHO have been distributed to the modelling team, and how the model comparison to the satellite data records has been initiated. In the next version of this document, due in cycle 2 of the project, this intermediate report will be updated to a full report on the outcome of the comparison between simulated and satellite-observed tropospheric NO_2 and HCHO data, their uncertainties, and the implications for the usefulness of the level-3 data generated for climate assessment.

1. Purpose and scope

1.1. Purpose

This document presents a preliminary assessment of the usefulness of NO_2 and HCHO (level-2 and level-3) data generated in the project for the purpose of climate assessment.

1.2. Scope

The scope of this version CAR is to report on lessons learned on using long-term satellite NO_2 and HCHO generated within this project (and its precursor QA4ECV) at ECMWF CAMS and the University of Toulouse for the purpose of climate assessment. This involves features of availability, coverage, consistency, completeness, uncertainty (propagation), and validation of the satellite data, and its usefulness for comparison against model simulations at timescales at which the climate, or aspects thereof, are noticeably changing.

We focus here on the following question relevant to climate modellers who evaluate their climate runs with satellite data records: *how can we better understand the causes of tropospheric O_3 trends in the tropics using ECV Precursor datasets through constraining precursor emissions in the GEOS-Chem model?*

1.3. Applicable documents

[AD-1] Data Standards Requirements for CCI Data Producers. Latest version at time of writing is v1.2: ref. CCI-PRGM-EOPS-TN-13-0009, 9 March 2015, available online at: https://climate.esa.int/media/documents/CCI_DataStandards_v2-3.pdf

[AD-2] CCI Data Policy v1.1. Available online at: https://climate.esa.int/sites/default/files/CCI_Data_Policy_v1.1.pdf

1.4. Reference documents

[RD-1] GCOS Climate Monitoring Principles, November 1999. Available online at: https://gcos.wmo.int/en/essential-climate-variables/about/gcos-monitoring-principles

[RD-2] Guideline for the Generation of Satellite-based Datasets and Products meeting GCOS Requirements, GCOS Secretariat, GCOS-128, March 2009 (WMO/TD No. 1488). Available online at: https://library.wmo.int/index.php?lvl=notice_display&id=12884#.Yw4rL7RByUk

[RD-3] Quality assurance framework for earth observation (QA4EO): http://qa4eo.org

[RD-4] The Global Observing System for Climate: Implementation Needs, GCOS-200, October 2016. Available online at: https://gcos.wmo.int/en/gcos-implementation-plan

[RD-5] Status of the Global Observing System for Climate, GCOS-195, October 2015. Available online at: https://library.wmo.int/index.php?lvl=notice_display&id=18962#.Yw4r8LRByUk

[RD-6] Hollmann, R., et al., The ESA climate change initiative: Satellite data records for essential climate variables. American Meteorological Society. Bulletin, Vol. 94, No. 10, 2013, p. 1541-1552.

[RD-7] Joint Committee for Guides in Metrology, 2008, Evaluation of measurement data — Guide to the expression of uncertainty in measurement (GUM), JGCM 100: 2008. Available online at: https://www.iso.org/sites/JCGM/GUM-JCGM100.htm

[RD-8] Merchant, C., et al., 2017, Uncertainty information in climate data records from Earth observation, Earth Syst. Sci. Data Discuss., vol. 9, p511-527

1.5. List of acronyms

AC-SAF	Satellite Application Facility on Atmospheric Composition Monitoring
ADP	Algorithm Development Plan
AK	Averaging Kernel
AMF	Air-mass factor
BB	Biomass-Burning
ATBD	Algorithm Theoretical Basis Document
BIRA-IASB	Royal Belgian Institute for Space Aeronomy
BIRA-IR	BIRA-IASB Infrared Team
BIRA-SYN	BIRA-IASB Synergy Team
BIRA-UVVIS	BIRA-IASB UV-Vis Team
BIRA-MOD	BIRA-IASB Tropospheric Modeling Team
CAMS	Copernicus Atmospheric Monitoring Service
C3S	Copernicus Climate Change Monitoring Service
CCI	ESA Climate Change Initiative
CCI+	Climate Change Initiative Extension (CCI+), is an extension of the CCI over the period 2017-2024.
CEDS	Community Emissions Data System
CEOS	Committee on Earth Observation Satellites
CMUG	Climate Modeling User Group
CO	Carbon monoxide
COBRA	COvariance-Based Retrieval Algorithm
CRDP	Climate Research Data Package
CRG	Climate Research Group
CTM	Chemistry Transport Model
DLR	German Aerospace Centre
DOAS	Differential Optical Absorption Spectroscopy
ECMWF	European Centre for Medium-range Weather Forecast

ECV	Essential Climate Variable
ENVISAT	Environmental Satellite (ESA)
EO	Earth Observation
EQAS	Equatorial Asia
ESA	European Space Agency
EU	European Union
EUMETSAT	European Organisation for the Exploitation of Meteorological Satellites
FCDR	Fundamental Climate Data Record
FINN	Fire INventory from NCAR
FRESCO	Fast Retrieval Scheme for Clouds from the Oxygen A band
FRM	Fiducial Reference Measurement
GCHP	GEOS-Chem High Performance
GCOS	Global Climate Observation System
GEOS-Chem	Goddard Earth Observing System Chemistry
GFED	Global Fire Emissions Database
GOME	Global Ozone Monitoring Instrument (aboard ERS-2)
GOME-2	Global Ozone Monitoring Instrument – 2 (aboard MetOp-A, -B and -C)
IASI	Infrared Atmospheric Sounding Interferometer
IGAC	International Global Atmospheric Chemistry
HEMCO	Harvard-NASA Emissions Component
HRI	Hyperspectral Range Index
KNMI	Royal Netherlands Meteorological Institute
LAERO	Laboratoire d'Aérologie
LEO	Low Earth Orbit
LUT	Look-up table
MEGAN	Model of Emissions of Gases and Aerosols from Nature
MERRA	Modern-Era Retrospective analysis for Research and Applications
Metop	Meteorological Operational Platform (EUMETSAT)
MOPITT	Measurement of Pollution in the Troposphere
NASA	National Aeronautics and Space Administration
NDACC	Network for the Detection of Atmospheric Composition Change
NHAF	Northern Hemisphere Africa
NH_3	Ammonia
NN	Neural Network
NO	Nitrogen monoxide
NOx	Nitrogen oxides
NO_2	Nitrogen dioxide
NRT	Near-Real Time
OCRA	Optical Cloud Recognition Algorithm)
OMI	Ozone Monitoring Instrument (aboard EOS-Aura)
O_3	Ozone
PCA	Principal Component Analysis
QA4ECV	Quality Assurance for Essential Climate Variables
QA4EO	Quality Assurance framework four Earth Observation
R&D	Research and Development

ROCINN	Retrieval of Cloud Information using Neural Networks
SAF	Satellite Application Facility
SCIAMACHY	Scanning Imaging Absorption Spectrometer for Atmospheric
SEAS	Southeast Asia
SHAF	Southern Hemisphere Africa
SHSA	Southern Hemisphere South America
S5P	Sentinel-5 Precursor
SoW	Statement of Work
STREAM	STRatospheric Estimation Algorithm from Mainz
SZA	Solar Zenith Angle
TEMIS	Tropospheric Emission Monitoring Internet Service
TENA	Temperate North America
TIR	Thermal Infrared spectral range
TROPOMI	Tropospheric Monitoring Instrument (aboard Sentinel-5 Precursor)
TOA	Top-of-atmosphere
TOAR-II	Tropospheric Ozone Assessment Report Phase-II
ULB	Université Libre de Bruxelles
IUP-UB	Institute of Environmental Physics, University of Bremen
UPAS	Universal Processor for UV/Vis Atmospheric Sensors
UV-Vis	Ultraviolet and visible spectral range
WP	Work Package

2. Evaluation of NO_2 and CO climate data records for ECMWF CAMS

ECMWF's CAMS system assimilates CO from MOPITT and IASI, and NO_2 from OMI (QA4ECV) and GOME-2 (AC-SAF) in their system. Apart from MOPITT CO, these are prototype data products retrieved in a manner consistent with the retrievals done in the ECV Precursor project. ECMWF's experience with these data records is therefore useful to take on board in the development and generation of the data records in this project.

2.1. Status of assimilation of satellite NO_2 in CAMS re-analysis

ECMWF recently tested (Autumn 2022) for the first time the assimilation of TROPOMI NO_2 (from KNMI) along with OMI (KNMI) and GOME-2B/C NO_2 (from AC-SAF) in its IFS system. Adding TROPOMI NO_2 to the assimilation reduces the bias over eastern Asia, where the CAMS system was known to be biased high previously (Figure 2.1 below). The impact of TROPOMI NO_2 assimilation is that it corrects for IFS model issues that led to too much NO_2 in forecast mode over China and the United States. The OMI and TROPOMI NO_2 retrieval approaches are very similar, and the data products agree well, but TROPOMI's spatial resolution and coverage are superior, so that assimilation of TROPOMI NO_2 has a proportionally stronger impact than OMI's.

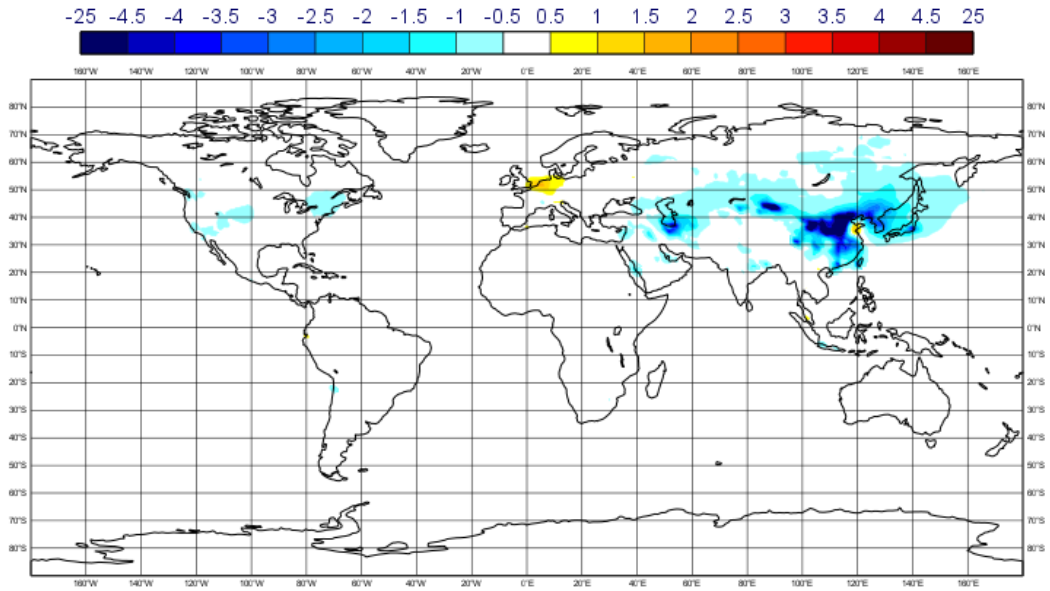

Figure 2.1 Difference in tropospheric NO_2 (ASSIM – CONTROL) when assimilating TROPOMI NO_2 along with OMI and GOME-2 NO_2 in ECMWF's IFS system vs. assimilating only OMI and GOME-2 NO_2.

In a project with KNMI, ECMWF is revisiting its assimilation approach. Instead of the previously used "thinning" approach, ECMWF is now experimenting with so-called 'superobservations'. Superobservations are averaged satellite data representative for the spatial domain of the model grid. An important advantage of superobservations is that they can be accompanied by realistic (gridded) uncertainty estimates that go beyond simple averaged uncertainties. ECMWF indicated that the ECV Precursor data would be more useful to them when filtering

criteria (e.g. solar zenith angle, qa_value, etc.) used in generating the level-3 data are included in the data products.

ECMWF is also testing a new assimilation scheme (4D-Var) in which NO_x emissions (rather than NO_2 columns) are updated based on the satellite NO_2 columns. Preliminary results indicate that the information added by the satellite data persists for a longer time in the assimilated fields, but there are also difficulties still (N. Bousserez, personal communication).

2.2. Status of assimilation of satellite CO in CAMS re-analysis

MOPITT and IASI-B/C CO are routinely assimilated into the CAMS re-analysis system (Inness et al., 2022). Validation revealed that CAMS CO (after assimilation) has a low bias of some 10% against ground based FTIR CO data collected from the NDACC network, and against TROPOMI CO columns. Assimilation of TROPOMI CO columns leads to an improved fit against IAGOS aicraft CO vertical profiles, especially in the lower troposphere. This suggests that IASI and MOPITT CO are not necessarily biased, but rather that the vertical sensitivity of TROPOMI to lower tropospheric CO (retrievals at 2.3 μm) is stronger than the vertical sensitivity of IASI (retrievals at) 4.7 μm which peaks in the middle troposphere. Continuation of IASI CO data in the CAMS system is foreseen, and the differences in vertical sensitivity between IASI and TROPOMI were anticipated and accounted for by application of the observation operator (averaging kernels) in the assimilation procedure.

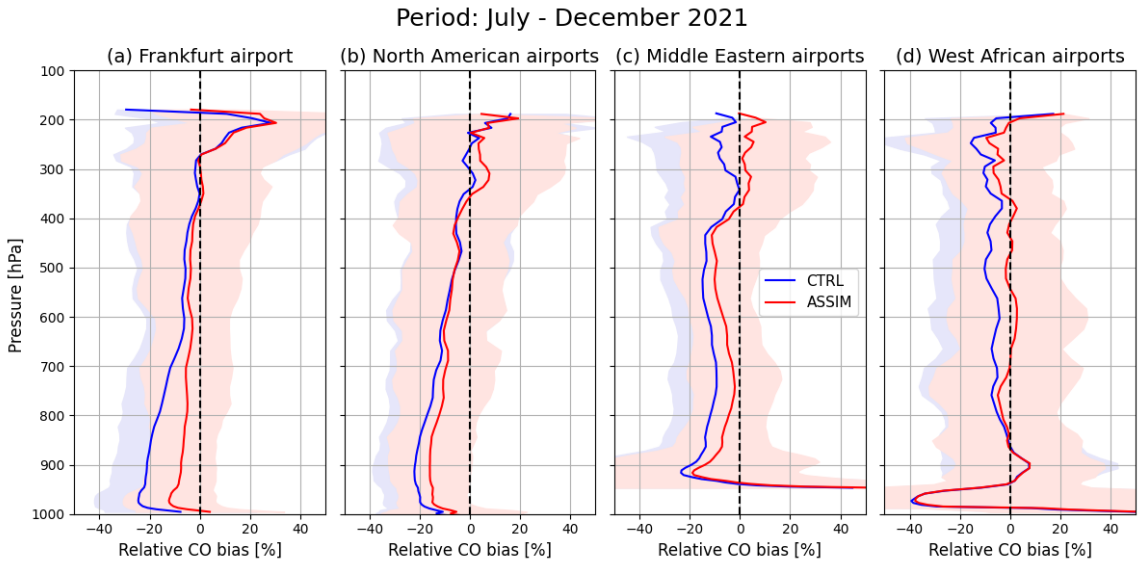

Figure 2.2. Comparison of CAMS CO biases against IAGOS CO profiles observed at various airports around the world. The red curves show the CAMS CO-profiles with the assimilation of TROPOMI CO columns, and the blue curves without the assimilation of TROPOMI CO. From Inness et al. (2022).

ECMWF will continue with the assimilation of IASI CO in its next reanalysis runs and is considering the usage of both nighttime and daytime IASI data. The IASI science team has advised ECMWF (Antje Inness) to assimilate both daytime and nighttime CO data, since both are of good scientific quality.

2.3. Perspective of assimilation of satellite HCHO in CAMS re-analysis

ECMWF is preparing the assimilation of satellite HCHO data in the IFS system (IFS documentation – Cy48r1, 2023) in the H2020 EU CAMEO-project (https://www.cameo-project.eu/), wherein BIRA (satellite remote sensing of HCHO), KNMI (chemistry in CAMS/IFS), and ECMWF (data assimilation) collaborate.

First technical data assimilation experiments in which CAMS HCHO concentrations were updated via HCHO satellite measurements were not successful. This was anticipated based on the short atmospheric lifetime of HCHO and the lessons learned with data assimilation of NO_2: information added to the system is quickly lost (within hours) after assimilation due to the short atmospheric lifetime of HCHO. The CAMEO-project is now at a stage in which a simplified chemical scheme describing the relationship between isoprene emissions and HCHO concentrations is being defined. With this simple scheme, it will be possible to assimilate (and perform inverse modelling) of satellite HCHO column data to update the isoprene emissions, a more long-lasting impact to the model. A first working version of the data assimilation system that updates isoprene emissions is anticipated by June 2024 (V. Huijnen – personal communication).

One of the lessons learned in working with the satellite data is that negative HCHO columns in the level-2 data should not be filtered out when constructing level-3 data (A. Inness, personal communication).

3. Preparation of GEOS-Chem simulations with constraints from HCHO and NO_2 climate data records

3.1. General objectives and motivation

Tropospheric ozone (O_3) is a harmful pollutant to human health (e.g. Brunekreef and Holgate, 2002; WHO, 2003; Bates, 2005) and control vegetation growth (Ainsworth et al., 2012; Monks et al., 2015). It is also a potent greenhouse gas particularly important in the upper troposphere (e.g. IPCC, 2007; Shindell et al., 2006; Stevenson et al., 2013). Tropospheric O_3 is produced by the photochemical oxidation of volatile organic compounds (VOCs) in the vicinity of nitrogen oxides (NO_x).

The time variation of tropospheric O_3 over the last few decades is characterised by significant regional variabilities. Gaudel et al. (2018) highlighted that tropospheric O_3 is the cause of the main discrepancies between observations and models, particularly in the tropics. Over the last 20 years, ozone precursor emissions have shifted from the mid-latitudes towards the equator (Zhang et al., 2016). In the tropics, anthropogenic emissions are increasing, especially in South-East Asia, and significant changes are expected in Africa as elsewhere.

The overall increase in O_3 in the troposphere therefore comes mainly from the tropics, although the interactions between emissions, transport and chemistry causing this increase remain poorly understood. As part of the Tropospheric Ozone Assessment Report Phase II (TOAR-II) initiative supported by the International Global Atmospheric Chemistry (IGAC), a working group on ozone and its precursors in the tropics has been set up to better understand the increase in tropical tropospheric O_3 (https://igacproject.org/opt-focusworking-group). Ozone and some of its precursors have been observed globally by space-based sensors for several decades. In particular, the tropospheric content of nitrogen dioxide (NO_2) and formaldehyde (HCHO) is documented by UV-Visible spectrometers such as GOME-2 (since 2006), OMI (2005-2021), and more recently TROPOMI (2018-now).

The Laboratoire d'Aerologie (LAERO) is involved in the TOAR-II working group Ozone and Precursors in the Tropics, which aims to determine the origin of the evolution of tropospheric O_3 and its precursors in the Tropics. LAERO is contributing to the ESA CCI+ Precursors project, concerning spaceborne observation of O_3 precursors (HCHO and NO_2) as essential climate variables (ECVs). LAEROs activity is to determine the impact of the evolution of surface emissions in the tropics upon the tropospheric O_3 through numerical simulations of the last decade with the GEOS-Chem chemistry transport model. The surface emission inventories from biomass burning and anthropogenic sources will be constrained using NO_2 and HCHO satellite observations from the ESA CCI+ consortium.

3.2. GEOS-chem model overview and strategy

3.2.1. GEOS-chem overview

The GEOS-Chem model is a global 3D Transport Chemistry Model (CTM) that has been used to analyse the sources and variabilities of atmospheric compositions (Whaley et al., 2015; Li et al., 2019; Hammer et al., 2020; Jiang et al., 2022). The GEOS-Chem model is driven by meteorological reanalysis data from the Goddard Earth Observing System (GEOS) of the Global Modelling and Assimilation Office (GMAO). We use the parallel version of GEOS-Chem called GEOS-Chem High Performance (GCHP), to run decadal simulations.

In the GEOS-Chem model, the emissions compound was configured using the Harvard-NASA Emissions Component (HEMCO) module (Keller et al., 2014; Li et al., 2021). We use GCHP v14.2.2 version (https://geoschem.github.io) with 72 vertical levels on a 2°x2.5° horizontal grid. For all our simulations the biogenic VOC emissions will come from the Model of Emissions of Gases and Aerosols from Nature (MEGAN) inventory (Guenther et al., 2012) and we use default emissions from other natural sources such as lightning, volcanoes, soil NO_x (Murray et al., 2012; Sauvage et al., 2007). The meteorological forcings come from Modern-Era Retrospective analysis for Research and Applications, version 2 (MERRA-2) reanalysis.

3.2.2. Strategy of model assessment

Emissions are the source of chemical species in the atmosphere and are therefore the starting point for modelling air composition. A simulation was carried out over the 2007-2021 period

without running the full chemistry in GCHP to check that the emissions are consistent with expected seasonal and long-term variations and with results from the literature.

This first simulation named “Emit_test1” uses anthropogenic emissions from the Community Emissions Data System (CEDS v2) (Hoesly et al., 2018) and BB emissions from the Global Fire Emissions Database or GFED v4 (Randerson et al., 2017). Then, a test was carried out including full chemistry for a first assessment of the simulated precursors distributions with the satellite products (ECVs). This report will show that these tests provided satisfactory results. Therefore, the reference (REF) full chemistry simulation will be performed with the CEDSv2 and GFEDv4 inventories for the 2007-2021 period. It will be evaluated thoroughly with the latest precursor (NO_2 and HCHO) satellite observations from the consortium: NO_2 tropospheric columns from UV-Visible sounders (OMI and TROPOMI) are provided by KNMI and HCHO by BIRA-IASB.

Once the assessment of this first full-chem simulation is performed, simulations without chemistry will be performed with FINN for BB and CAMS-GLOB-ANT for anthropogenic emission. The validation of the REF simulation with satellite observations will provide a constraint for the choice of the best couple of emission inventories. We will compute differences of NO_2 and HCHO distributions from simulations without chemistry for the different couple of inventories. The spatio-temporal consistency between REF versus observations and inventories differences will indeed provide a constraint to select the couple (BB and anthropogenic) of inventories that are the most likely to correct the model biases.

3.3. Preliminary evaluation

3.3.1. Global NO_x emissions and interannual variation

Nitrogen oxides (NO_x) are chemical compounds that are both emitted and formed in the troposphere. NO_x is mainly composed of nitrogen monoxide (NO) and nitrogen dioxide (NO_2). NO_x emissions are mainly in the form of NO and come from natural sources (soil and lightnings) and anthropogenic sources through the combustion of fossil fuels or biomass, aircraft and shipping. NO_2 is a pollutant that has an impact on air quality through its toxic effect on health. NO_2 is also a precursor gas for ozone, which is itself toxic. The NOx emissions from our simulation “Emit_test1” by source (e.g. soil, lightning, biomass burning, anthropogenic) are represented and illustrated in the figure 3.3.1. NO_x emissions from aircraft and ships are not presented here as they do not display clear seasonal variations.

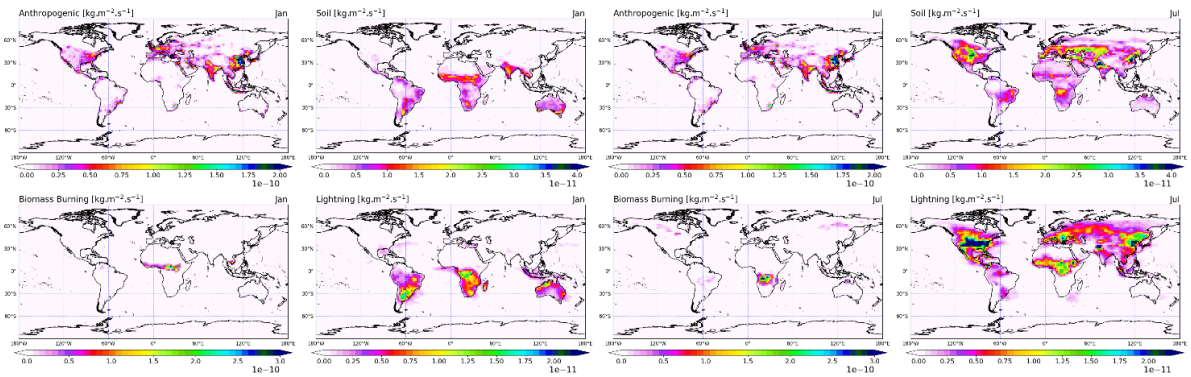

Figure 3.3.1: NOx emission averaged over all January (left) and July (right) from 2010 to 2021: anthropogenic, soil, biomass-burning and lightning.

Figure 3.3.1 shows that NO_x anthropogenic emissions are mainly produced in China, temperate North America and Europe. Figure 3.3.1 also reveals that the seasonal variability of lightning and soil NO_x emissions are consistent with what is expected. Lightning NO_x emission occur mainly during the wet seasons, i.e. in January in the Southern Hemisphere and in July in the Northern Hemisphere. BB emissions are logically occurring during the dry season, with the most intense emissions in January in the Northern Hemisphere and in July in the Southern Hemisphere in Africa.

We have also checked the temporal evolution of emissions. Figure 3.3.2 presents the global NO_x emissions for different sources in Tg N yr^{-1} from 2010 to 2021. The left panel of the figure 3.3.2 shows the global NO_x emissions from various sources, while the right panel shows the anthropogenic NO_x emissions for major emitting regions such as China (solid cyan line), TENA (dotted cyan line) and Europe (dashed cyan line).

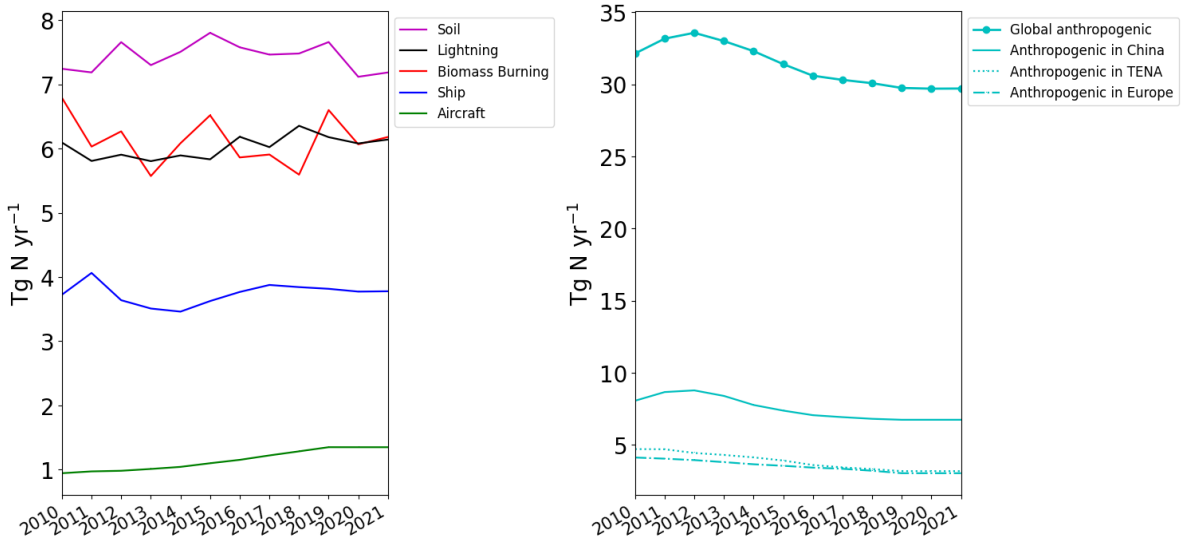

Figure 3.3.2: Temporal evolution of the global NO_x emissions from soil, lightning, biomass burning, ship, aircraft (left) and anthropogenic (right) and in Tg N yr^{-1} from 2010 to 2021 Lightning, soil, BB and ship emissions do not display significant temporal trends.

Anthropogenic NO_x emissions are clearly decreasing in the 2010 in NA and Europe and since 2012 in China. The decrease in NO_x over China since 2012 has been largely documented and is resulting in a coincident decrease of tropospheric NO_2 columns over China as detailed in Zhang et al. (2024). We note finally that NO_x anthropogenic emissions evolution is in good agreement with McDuffie et al (2020) in term of variations.

Table 3.3.1 shows that NOx biomass burning emission from GEOS-Chem is similar to Bray et al., (2020). Similarly, GEOS-Chem NO_x soil emissions are very close to Weng et al., (2020). Annual lightning NO_x emissions are consistent with those of Murray (2006). GC aircraft NO_x emissions are similar to that reported by Quadros et al., (2022) and finally, NO_x emissions from

ships are significantly lower than in IMO (2015) and Burgard and Bria (2016) but remains reasonable in terms of order of magnitude.

Table 3.3.1 Comparison of NO_x emissions from GEOS-Chem with the literature

Source	GEOS-Chem [Tg Nyr^{-1}]	References [Tg Nyr^{-1}]
Biomass-burning	6.1	6.8 (Bray et al., 2020)
Soil	7.4	7.5 (Weng et al., 2020)
Aircrafts	1.3	1.6 (Qudros et al., 2022)
Anthropogenic	31.3	33 (McDuffie et al., 2020)
Lightning	6	2-8 (Murray, 2016)
Ships	3.7	6.3 (IMO, 2015; Burgard and Bria, 2016)

The analysis of inter-annual variations in NO_x emissions from different sources on a global scale has shown that the GFED4 BB emissions and the CEDs v2 anthropogenic emissions are in very good agreement with the literature in terms of magnitude. The long-term evolution of the global anthropogenic NO_x emissions is also in very good agreement with McDuffie et al., (2020).

3.3.2. Subdomain seasonal variation

We now examine the seasonal variability of the different sources of NO_x for different regions of the globe. Figure 3.3.3 displays the different domains we have selected for detailed analysis of NOx emissions variability.

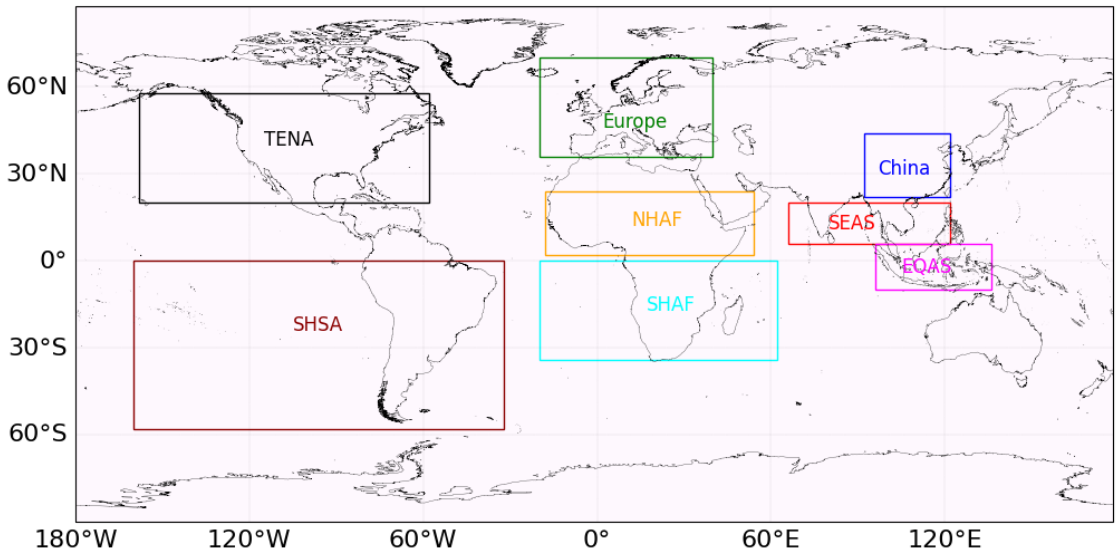

Figure 3.3.3: Subdomain for the different region of NOx emission analysis. Temperate North America (TENA) Southern Hemisphere South America (SHSA), Northern Hemisphere Africa (NHAF), Southern Hemisphere Africa (SHAF), Southeast Asia (SEAS), Equatorial Asia (EQAS).

3.3.2.1. Southern Hemisphere South America (SHSA) subdomain

The seasonal variabilities of NO_x emissions [Tg $Nmonth^{-1}$] from biomass-burning, soil and lightning over SHSA are presented in Figure 3.3.4.

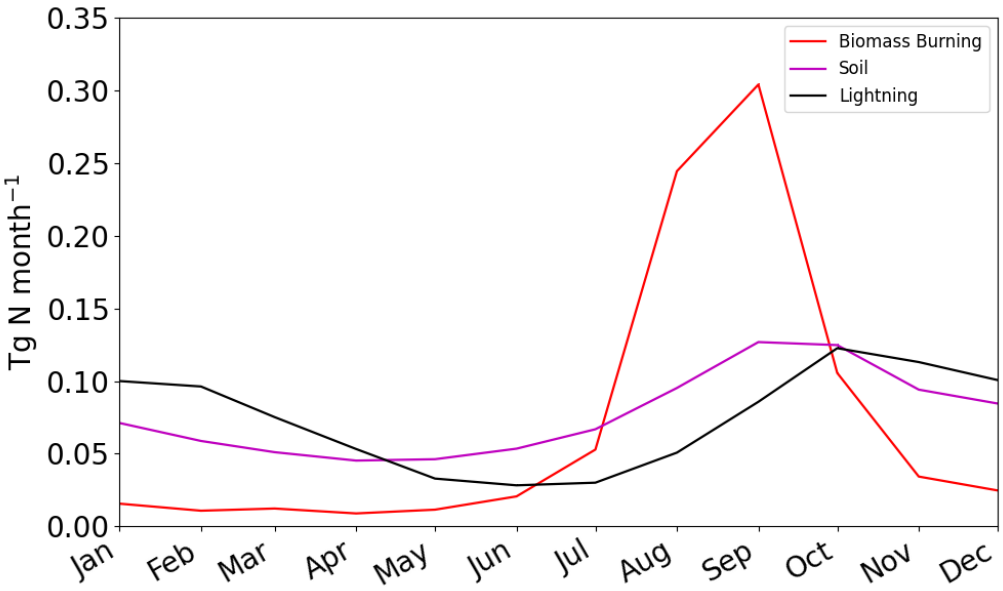

Figure 3.3.4 Seasonal variability of NO_x emissions (lightning, Soil and biomass-burning) in [Tg N month^{-1}] over SHSA.

NO_x emissions from BB (red line) shows a strong seasonal variability, with the highest values occurring during the fire season (August- September). The seasonal variations of NOx from biomass burning are consistent with the organic carbon (OC) seasonal variations reported in Pan et al. (2020). Complementary to BB, Lightning NO_x emissions are maxima during the October to February period corresponding to the wet season. NOx emissions from soil are the highest in September. The temporal evolution of other sources of NO_x is not mentioned because they are much smaller and do not present significant variations.

3.3.2.2. Temperate North America, Europe and China domain

In this section we have present emissions from the three (03) regions with the highest NO_x anthropogenic emissions: TENA, Europe and China. Figure 3.3.5 shows China (solid cyan line) is the largest NO_x emitter. In the three regions, NO_x anthropogenic emission are maxima in winter because of domestic heating. The secondary peak in summer in China and TENA is probably related to air coolers.

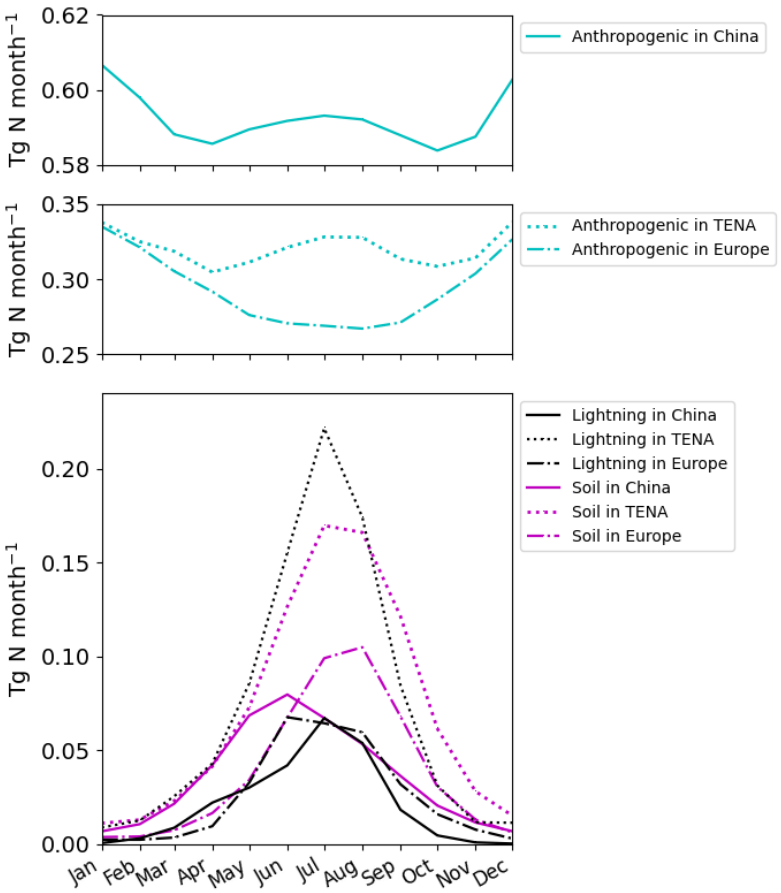

Figure 3.3.5 Seasonal variability of NO_x emissions in Tg N month^{-1}. Top figure shows anthropogenic emissions in China, the middle figure represents the anthropogenic NO_x for TENA and Europe and the bottom figure shows Lightning and soil emissions in TENA, Europe and China.

NO_x Lightning Emissions in TENA are higher than in the other regions, with a logical peak in summer (JJA) TENA also emits larger quantities of soil NO_x than China and Europe with a maximum also occurring in summer.

3.3.2.3. Equatorial Asia (EQAS) and South Est Asia (SEAS) domains

In EQAS (Figure 3.3.6, left), emissions from BB logically occur during the August-September-October period with a peak around 0.1 Tg N in September; Lightning emissions, display little seasonal variability as expected in the equatorial region less marked by strong seasonal weather variations than the tropics and mid-latitudes. For the SEAS region (Figure 3.3.6, right), soil NO_x emissions are the highest in MAM (peak on April) caused probably by the monsoon season. BB NOx are maxima during the February to April period with a peak 0.1 Tg N in March. BB NO_x emission in SEAS is greater than in EQAS because of SEAS has a relatively cooler dry season than EQAS region.

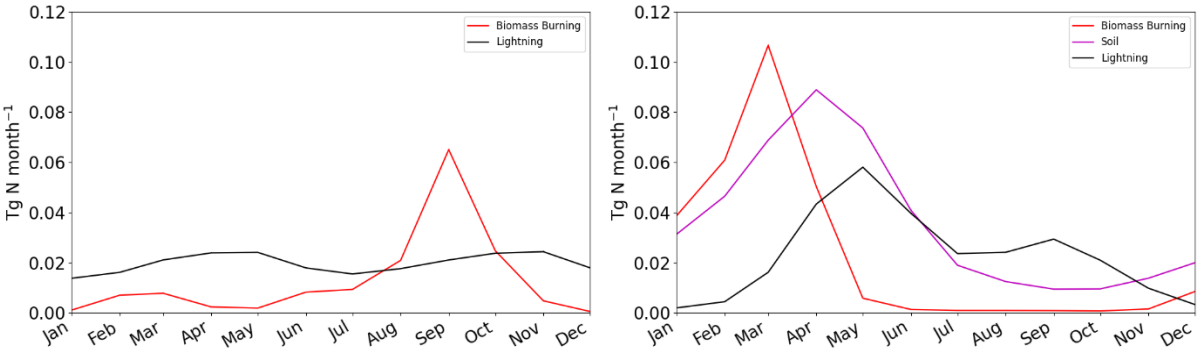

Figure 3.3.6 Seasonal variability of NO_x emissions in EQAS (left panel) and SEAS region (right panel).

3.3.2.4. Northern Hemisphere Africa (NHAF) and Southern Hemisphere Africa domains (SHAF)

Figure 3.3.7 clearly shows that $LiNO_x$ emissions are the highest during JJA for NHAF while it is greater on DJF in SHAF region as expected from the respective rainy seasons.

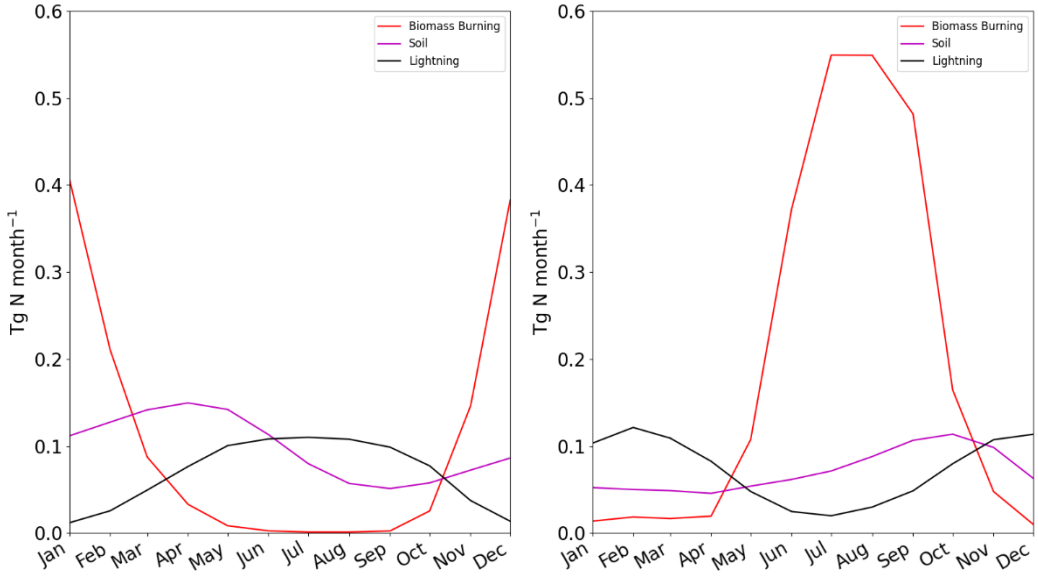

Figure 3.3.7 Seasonal variability of NOx emissions (lightning, Soil and biomass-burning) in Tg N month^{-1} in NHAF (left) and SHAF (right)

Soil NO_x emissions are occurring in spring, MAM in NHAF and SON in the SHAF region because of N-availability and humidity of soils. In the other words, Soil NO_x depends heavily on climate and edaphic conditions, and are most strongly correlated with temperature, precipitation patterns, and fertilizer policy practices. BB NO_x emissions are of course maxima during the dry seasons, JJA in the SHAF and DJF in NHAF. BB NO_x emissions are larger in SHAF than in NHAF and even larger than in all regions discussed previously, with a peak of around 0.55 Tg N.

3.3.3. Assessment of the 3D GEOS-Chem model

3.3.3.1. Report on the meeting with BIRA and KNMI on HCHO and NO_2 dataset

A meeting was held with LAERO, BIRA-IASB and KNMI at the beginning of January 2023 to discuss the satellite products to be used in the project. These satellite products are required and important to validate our GEOS-Chem simulations. As part of the project, the tropospheric NO_2 columns from GEOS-Chem will be compared with the satellite products provided by KNMI, such as the retrievals from OMI (2007-2021) and TROPOMI (2018-2021).
For formaldehyde (HCHO), the tropospheric HCHO columns from GEOS-Chem will be compared with the HCHO columns from TROPOMI, which are provided by BIRA-IASB. And finally, the tropospheric ozone columns will be compared to IASI-SOFRID (LAERO) tropospheric ozone columns. KNMI and BIRA-IASB provided the satellite data for the requested period and at the same horizontal resolution as the GEOS-Chem simulations (2°x2.5°). We only present comparisons of OMI tropospheric NO_2 distributions (KNMI) and GEOS-Chem in this report. The short test full chemistry simulation that has been performed for January-February 2010 and TROPOMI was launched in 2018. We have therefore compared HCHO simulated distributions with OMI retrievals, from the TEMIS database (https://www.temis.nl/).

3.3.3.2. Comparison of the tropospheric columns of HCHO and NO_2 simulated and observed

a) HCHO Tropospheric column

HCHO contributes to the photochemical formation of tropospheric O_3. Although HCHO itself is not a major greenhouse gas, it does contribute indirectly to climate change by reacting in the atmosphere to form compounds that affect the climate.

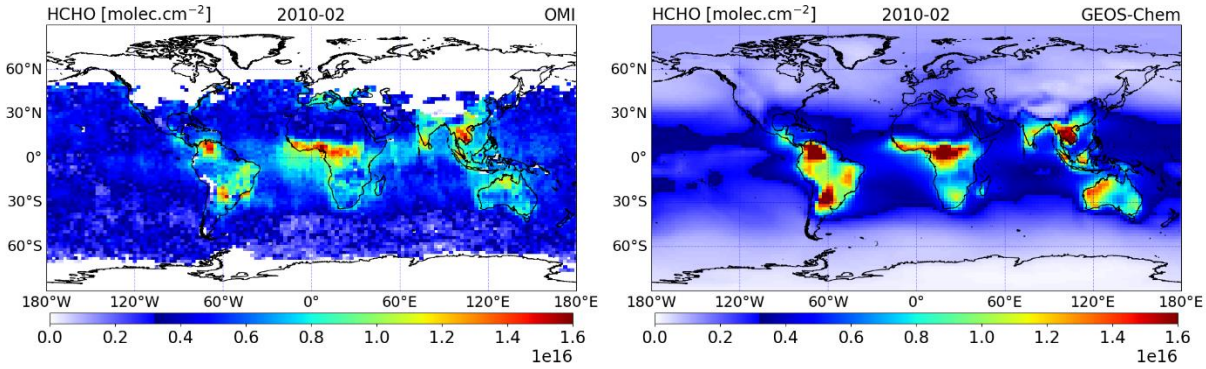

Figure 3.3.8 Tropospheric HCHO columns from OMI (left) and from GEOS-Chem (right)

Figure 3.3.8 presents the HCHO tropospheric columns retrieved from OMI (left panel) and simulated by GEOS-Chem (right panel) on February 2010. HCHO tropospheric columns from OMI and GC have similar structures with a similar order of magnitude (1E+16 molec.cm^{-2}). The maxima of the tropospheric columns from OMI and GC are located over the same regions (e.g. Indochina peninsula, SHSA, NHAF). The highest values are related to the presence of large biogenic emissions (e.g. isoprene).

b) NO_2 tropospheric column:

Figure 3.3.9, presents the distributions of OMI (KNMI) and GC NO_2 tropospheric columns for February 2010. For OMI, North Hemisphere latitudes above 40°N are lacking (due to snow and ice coverage) which is not allowing us to make a complete comparison.

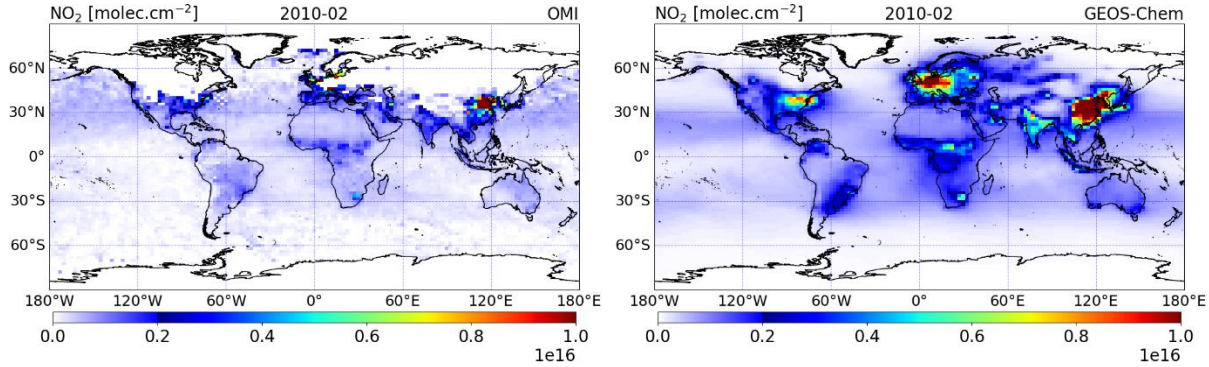

Figure 3.3.9 Tropospheric NO_2 columns from OMI (left) and from GEOS-Chem (right)

The OMI distribution has a pattern similar to GEOS-Chem. However, GC tropospheric NO_2 columns are generally larger than OMI's columns. As expected, the GC maxima are located over the largest emission regions which are China, TENA and Europe. The main objective of the LAERO activity in the ESA-CCI+ project is to understand the causes of the tropospheric O3 trends in the tropics using ECV's to constrain precursor emissions in the model. We will therefore use IASI-SOFRID satellite retrievals from LAERO to evaluate the simulated O_3 distributions.

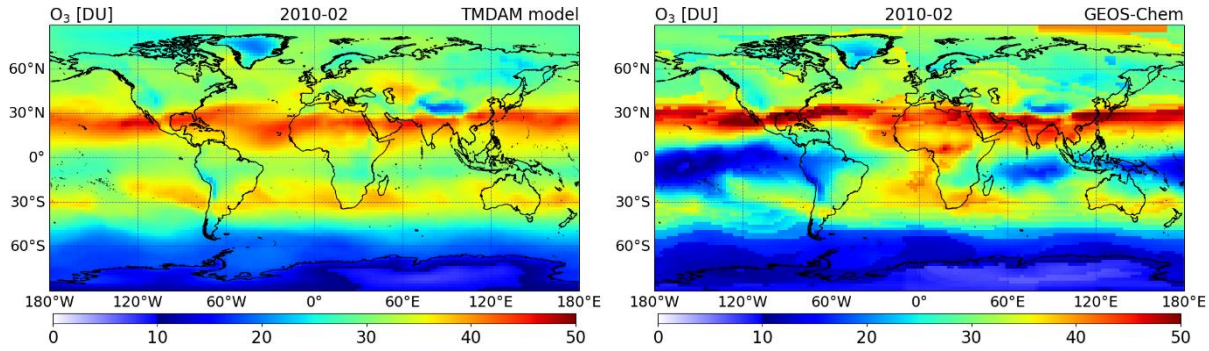

Figure 3.3.10 Tropospheric O_3 columns from TMDAM (left) and from GEOS-Chem (right)

Figure 3.3.10 displays a preliminary example of comparison of GC tropospheric O_3 columns with satellite-based data (OMI/GOME-2A, L4 processor: TMDAM, level2-processor: OPERA v.1.36, Jacob et al., 2018). It clearly shows that the distribution of tropospheric O_3 columns from GEOS-Chem agrees very well with the assimilated data.

The evaluation of the long-term model simulation will be made with the IASI-SOFRID tropospheric O_3 columns taking into account the satellite retrievals vertical sensitivity.

3.4. Conclusion and future work

At LAERO we have setup the GC model for a full chemistry long-term (2007-2021) simulation. We have first performed a test simulation without chemistry to check the consistency of the default emissions (GFED4 for biomass burning and CEDS v2 for anthropogenic) of the model. The results of this test first shows that the global interannual variability and the annual mean emissions from the different sources are in agreement with the literature. For instance, with CEDSv2, China is the largest NO_x emitter and displays a decrease of emissions since 2011-2012 as reported. We noted also that seasonal variabilities agree with what is expected in the different regions (maximum anthropogenic emissions in winter in Europe, maximum biomass burning NO_x emission during dry seasons, soil and lightnings mostly during wet seasons).

The second part of this work has been to branch the chemistry mechanism and running a two-month simulation using the "Emit_test1" configuration as input in the model. The general pattern of the NO_2 and HCHO tropospheric column distributions from GEOS-Chem are in good agreement with OMI retrievals. The amplitude of variations is very similar for HCHO and slightly overestimated for NO_2.

The tropospheric O_3 columns from our preliminary GC simulations are also consistent with assimilated data (OMI/GOME-2A, Level 4 processor: TMDAM, level2-processor) with very similar patterns.

Now that we have performed a sanity check on our emissions and performed a successful preliminary short fullchem run we will run a fullchem reference simulation for the 2007-2010 period with GFED4 BB and CEDS v2 anthropogenic emissions. The comparisons of the NO_2 and HCHO simulated distributions with the latest NO_2 and HCHO ECVs from the ESA-CCI+ consortium will provide the constraint for the choice of an optimal set of BB and anthropogenic emissions. We will use this satellite constrained simulation to determine the impact of changing emissions on the evolution of tropospheric O_3 in the tropics.

4. References

Ainsworth, E., Yendrek, C., Sitch, S., Collins, W., and Emberson, L.: The Effects of Tropospheric Ozone on Net Primary Productivity and Implications for Climate Change, Annu. Rev. Plant Biol., 63, 637–661, https://www.annualreviews.org/doi/10.1146/annurev-arplant-042110-103829, 2012

Bates, David V.. Ambient Ozone and Mortality. Epidemiology 16, 427-429, DOI: 10.1097/01.ede.0000165793.71278.ec, 2005

Brunekreef, B. and Holgate, S. T.: Air pollution and health, The Lancet, 360, 1233–1242, 2002.

Bray, C. D., Battye, W. H., Aneja, V. P., & Schlesinger, W. H. (2021). Global emissions of NH3, NOx, and N2O from biomass burning and the impact of climate change. *Journal of the Air & Waste Management Association*, *71*(1), 102–114. https://doi.org/10.1080/10962247.2020.1842822

Burgard, D. A. and Bria, C. R.: Bridge-based sensing of NO_x and SO_2 emissions from ocean-going ships, Atmospheric Environment, 136, 54–60, https://doi.org/https://doi.org/10.1016/j.atmosenv.2016.04.014, 2016.

Gaudel, A., Cooper, O. R., Ancellet, G., Barret, B., Boynard, A., Burrows, J. P., Clerbaux, C., Coheur, P. F., Cuesta, J., Cuevas, E., Doniki, S., Dufour, G., Ebojie, F., Foret, G., Garcia, O., Granados-Munoz, M. J., Hannigan, J. W., Hase, F., Hassler, B., Huang, G., Hurtmans, D., Jaffe, D., Jones, N., Kalabokas, P., Kerridge, B., Kulawik, S., Latter, B., Leblanc, T., Le Flochmoen, E., Lin, W., Liu, J., Liu, X., Mahieu, E., McClure-Begley, A., Neu, J. L., Osman, M., Palm, M., Petetin, H., Petropavlovskikh, I., Querel, R., Rahpoe, N., Rozanov, A., Schultz, M. G., Schwab, J., Siddans, R., Smale, D., Steinbacher, M., Tanimoto, H., Tarasick, D. W., Thouret, V., Thompson, A. M., Trickl, T., Weatherhead, E., Wespes, C., Worden, H. M., Vigouroux, C., Xu, X., Zeng, G., and Ziemke, J.: Tropospheric Ozone Assessment Report: Present-day distribution and trends of tropospheric ozone relevant to climate and global atmospheric chemistry model evaluation, Elem. Sci. Anthrop., 6, 39, https://doi.org/10.1525/elementa.291, 2018.

Guenther, A., Karl, T., Harley, P., Wiedinmyer, C., Palmer, P. I., and Geron, C.: Estimates of global terrestrial isoprene emissions using MEGAN (Model of Emissions of Gases and Aerosols from Nature), Atmos. Chem. Phys., 6, 3181–3210, https://doi.org/10.5194/acp-6-3181-2006, 2006.

Hammer, M. S., van Donkelaar, A., Li, C., Lyapustin, A., Sayer, A. M., Hsu, N. C., Levy, R. C., Garay, M. J., Kalashnikova, O. V., Kahn, R. A., Brauer, M., Apte, J. S., Henze, D. K., Zhang, L., Zhang, Q., Ford, B., Pierce, J. R., and Martin, R. V. : Global Estimates and Long-Term Trends of Fine Particulate Matter Concentrations (1998–2018), Environ. Sci. Technol., 54, 7879–7890, https://doi.org/10.1021/acs.est.0c01764 , 2020.

Hoesly, R. M., Smith, S. J., Feng, L., Klimont, Z., Janssens Maenhout, G., Pitkanen, T., Seibert, J. J., Vu, L., Andres, R. J., Bolt, R. M., Bond, T. C., Dawidowski, L., Kholod, N., Kurokawa, J.-I., Li,

M., Liu, L., Lu, Z., Moura, M. C. P., O'Rourke, P. R., and Zhang, Q.: Historical (1750–2014) anthropogenic emissions of reactive gases and aerosols from the Community Emissions Data System (CEDS), Geosci. Model Dev., 11, 369–408, https://doi.org/10.5194/gmd-11-369-2018, 2018.

IFS Documentation – Cy48r1, Part VIII: Atmospheric Composition, ECMWF, 27 June 2023.

IMO, 2015. Third IMO GHG Study 2014. WWW Document. accessed 1.7.16. http://www.imo.org/en/ourwork/environment/pollutionprevention/airpollution/pages/greenhouse-gas-studies-2014.aspx .

Inness, A., Aben, I., Ades, M., Borsdorff, T., Flemming, J., Jones, L., Landgraf, J., Langerock, B.,Nedelec, P., Parrington, M., and Ribas, R.: Assimilation of S5P/TROPOMI carbon monoxide data with the global CAMS near-real-time system, Atmos. Chem. Phys., 22, 14355–14376, https://doi.org/10.5194/acp-22-14355-2022, 2022.

IPCC: Climate Change 2007: The Physical Science Basis. Contribution of Working Group I to the Fourth Assessment Report of the Intergovernmental Panel on Climate Change. Chapter 1, Historical Overview of Climate change, in: Intergovernmental Panel on Climate Change Climate change: The Physical Science Basis, Contribution of Working Group I to the Fourth Assessment Report of the IPCC, Cambridge University Press, Cambridge, 79–131, 2007.

Jiang, Z., Zhu, R., Miyazaki, K., McDonald, B. C., Klimont, Z., Zheng, B., Boersma, K. F., Zhang, Q., Worden, H., Worden, J. R., Henze, D. K., Jones, D. B. A., Denier van der Gon, H. A. C., and Eskes, H.: Decadal Variabilities in Tropospheric Nitrogen Oxides Over United States, Europe, and China, J. Geophys. Res.-Atmos., 127, e2021JD035872, https://doi.org/10.1029/2021jd035872, 2022.

Keller, C. A., Long, M. S., Yantosca, R. M., Da Silva, A. M., Pawson, S., and Jacob, D. J.: HEMCO v1.0: a versatile, ESMF-compliant component for calculating emissions in atmospheric models, Geosci. Model Dev., 7, 1409–1417, https://doi.org/10.5194/gmd-7-1409-2014 , 2014.

Li, K., Jacob, D. J., Liao, H., Shen, L., Zhang, Q., and Bates, K. H.: Anthropogenic drivers of 2013-2017 trends in summer surface ozone in China, P. Natl. Acad. Sci. USA, 116, 422–427, https://doi.org/10.1073/pnas.1812168116 , 2019.

Lin, H., Jacob, D. J., Lundgren, E. W., Sulprizio, M. P., Keller, C. A., Fritz, T. M., Eastham, S. D., Emmons, L. K., Campbell, P. C., Baker, B., Saylor, R. D., and Montuoro, R.: Harmonized Emissions Component (HEMCO) 3.0 as a versatile emissions component for atmospheric models: application in the GEOS-Chem, NASA GEOS, WRF-GC, CESM2, NOAA GEFS-Aerosol, and NOAA UFS models, Geosci. Model Dev., 14, 5487–5506, https://doi.org/10.5194/gmd-14-5487-2021, 2021.

McDuffie, E. E., Smith, S. J., O'Rourke, P., Tibrewal, K., Venkataraman, C., Marais, E. A., Zheng, B., Crippa, M., Brauer, M., and Martin, R. V. : A global anthropogenic emission inventory of atmospheric pollutants from sector- and fuel-specific sources (1970–2017): an application of the Community Emissions Data System (CEDS), Earth Syst. Sci. Data, 12, 3413–3442, https://doi.org/10.5194/essd-12-3413-2020, 2020.

Monks, PS, Archibald, AT, Colette, A, Cooper, O, Coyle, M, Derwent, R, Fowler, D, Granier, C, Law, KS, Mills, GE, Stevenson, DS, Tarasova, O, Thouret, V, von Schneidemesser, E, Sommariva, R, Wild, O and Williams, ML. 2015. Tropospheric ozone and its precursors from the urban to the global scale from air quality to short-lived climate forcer. Atmos. Chem. Phys., 15, 8889–8973, DOI: https://doi.org/10.5194/acp-15-8889-2015, 2015.

Murray, L.T. Lightning NO*x* and Impacts on Air Quality. *Curr Pollution Rep* 2, 115–133 (2016). https://doi.org/10.1007/s40726-016-0031-7

Murray, L. T., Jacob, D. J., Logan, J. A., Hudman, R. C., and Koshak, W. J.: Optimized regional and interannual variability of lightning in a global chemical transport model constrained by LIS/OTD satellite data, J. Geophys. Res., 117, D20307, https://doi.org/10.1029/2012JD017934, 2012

Jacob C. A. van Peet, Ronald J. van der A, Hennie M. Kelder, and Pieternel F. Levelt (2018), Simultaneous assimilation of ozone profiles from multiple UV-VIS satellite instruments, Atmospheric Chemistry and Physics, https://doi.org/10.5194/acp-18-1685-2018

Pan, X., Ichoku, C., Chin, M., Bian, H., Darmenov, A., Colarco, P., Ellison, L., Kucsera, T., da Silva, A., Wang, J., Oda, T., and Cui, G.: Six global biomass burning emission datasets: intercomparison and application in one global aerosol model, Atmos. Chem. Phys., 20, 969–994, https://doi.org/10.5194/acp-20-969-2020, 2020.

Quadros, F. D., Snellen, M., and Dedoussi, I. C.: Recent and Projected Trends in Global Civil Aviation Fleet Average NOx Emissions Indices, https://doi.org/10.2514/6.2022-2051.

Randerson, J.T., G.R. van der Werf, L. Giglio, G.J. Collatz, and P.S. Kasibhatla. 2017. Global Fire Emissions Database, Version 4.1 (GFEDv4). ORNL DAAC, Oak Ridge, Tennessee, USA. https://doi.org/10.3334/ORNLDAAC/1293

Sauvage, B., Martin, R. V., van Donkelaar, A., Liu, X., Chance, K., Jaeglé, L., Palmer, P. I., Wu, S., and Fu, T.-M.: Remote sensed and in situ constraints on processes affecting tropical tropospheric ozone, Atmos. Chem. Phys., 7, 815–838, https://doi.org/10.5194/acp-7-815-2007, 2007

Shindell, D. T., Faluvegi, G., and Stevenson, D. S. E. A.: Multimodel simulations of carbon monoxide: Comparison with observations and projected near-future changes, J. Geophys. Res.-Atmos., 111, D19306, https://doi.org/10.1029/2006jd007100, 2006.

Stevenson, D. S., Young, P. J., Naik, V., Lamarque, J.-F., Shindell, D. T., Voulgarakis, A., Skeie, R. B., Dalsoren, S. B., Myhre, G., Berntsen, T. K., Folberth, G. A., Rumbold, S. T., Collins, W. J., MacKenzie, I. A., Doherty, R. M., Zeng, G., van Noije, T. P. C., Strunk, A., Bergmann, D., Cameron-Smith, P., Plummer, D. A., Strode, S. A., Horowitz, L., Lee, Y. H., Szopa, S., Sudo, K., Nagashima, T., Josse, B., Cionni, I., Righi, M., Eyring, V., Conley, A., Bowman, K. W., Wild, O., and Archibald, A.: Tropospheric ozone changes, radiative forcing and attribution to emissions in the Atmospheric Chemistry and Climate Model Intercomparison Project (ACCMIP), Atmos. Chem. Phys., 13, 3063–3085, doi:10.5194/acp-13-3063-2013, 2013.

Weng, H., Lin, J., Martin, R. *et al.* Global high-resolution emissions of soil NOx, sea salt aerosols, and biogenic volatile organic compounds. *Sci Data* 7, 148 (2020). https://doi.org/10.1038/s41597-020-0488-5

Whaley, C. H., Strong, K., Jones, D. B. A., Walker, T. W., Jiang, Z., Henze, D. K., Cooke, M. A., McLinden, C. A., Mittermeier, R. L., Pommier, M., and Fogal, P. F.: Toronto area ozone: Long-term measurements and modeled sources of poor air quality events, J. Geophys. Res.-Atmos., 120, 11368–11390, https://doi.org/10.1002/2014JD022984, 2015.

WHO: Health Aspects of Air Pollution with Particulate Matter, Ozone and Nitrogen Dioxide, Bonn, 2003.

Zhang, Y, Cooper, OR, Gaudel, A, Thompson, AM, Nédélec, P, Ogino, S-Y and West, JJ. Tropospheric ozone changes from 1980 to 2010 dominated by equatorward redistribution of emissions. *Nature Geosci.,* 9, 875–879, https://doi.org/10.1038/ngeo2827, 2016

Zhang Y, Chen L, Guo W, Zhou C and Li Z (2024), The variability of NO_2 concentrations over China based on satellite and influencing factors analysis during 2019–2021. Front. Environ. Sci. 12:1267627. doi: 10.3389/fenvs.2024.1267627